Metabolomic signatures in lipid-loaded HepaRGs reveal pathways involved in steatotic progression

MV Brown[1,*], **SA Compton**[2,*], **MV Milburn**[1], **KA Lawton**[1], and **B Cheatham**[2]

[1]Metabolon, Inc. 617 Davis Drive, Suite 400, Durham, NC, 27713, USA

[2]ZenBio 3200 East Highway 54, Suite 100, Research Triangle Park, NC, 27709 USA

Abstract

Objectives—Non-alcoholic fatty liver disease (NAFLD) describes a spectrum of disorders including simple steatosis, non-alcoholic steatohepatitis, fibrosis, and cirrhosis. With the increased prevalence of obesity, and consequently NAFLD, there is a need for novel therapeutics in this area. To facilitate this effort, we developed a cellular model of hepatic steatosis using HepaRG cells and determined the resulting biochemical alterations.

Design and methods—Using global metabolomic profiling, by means of a novel metabolite extraction procedure, we examined the metabolic profiles in response to the saturated fatty acid palmitate, and a mixture of saturated and unsaturated fatty acids, palmitate and oleate (1:2).

Results—We observed elevated levels of the branched chain amino acids, TCA cycle intermediates, sphingosine and acylcarnitines, and reduced levels of carnitine in the steatotic HepaRG model with both palmitate and palmitate:oleate treatments. In addition, palmitate-induced steatotic cells selectively displayed elevated levels of diacylglycerols and monoacylglycerols, as well as altered bile acid metabolism.

Conclusion—This global metabolomics approach reveals biochemical changes in pathways important in the transition to hepatic steatosis including insulin resistance, altered mitochondrial metabolism, and oxidative stress. Moreover, our data demonstrate the utility of this *in vitro* model for investigating mechanisms of steatotic progression, insulin resistance and lipotoxicity in NAFLD.

Keywords

Steatosis; metabolomics; lipid; liver; hepatocyte; NAFLD; NASH

Corresponding author: Bentley Cheatham, ZenBio 3200 East Highway 54, Suite 100, Research Triangle Park, NC, 27709 USA. Telephone: (919) 547-0692. Fax: (919) 547-0693. bentley@zenbio.com.
*These authors contributed equally to the work
Reprint requests: Bentley Cheatham, ZenBio 3200 East Highway 54, Suite 100, Research Triangle Park, NC, 27709 USA

Introduction

In parallel with the increasing occurrence of obesity and type 2 diabetes, non-alcoholic fatty liver disease (NAFLD) may be affecting up to 25% of the general population, including a significant portion of pediatric cases (1, 2). Current predictions indicate that 40% of the population will be obese by 2025 with NAFLD becoming the leading cause of liver disease and need for liver transplantation (3). While the exact mechanisms are not completely understood, excess lipid accumulation in hepatocytes is a primary event in the development of NAFLD.

Hepatic free fatty acids (FFAs) are derived from multiple sources including *de novo* synthesis, adipose tissue, and dietary triglycerides (4). In the liver, FFAs are converted to fatty acyl CoAs which are directed to specific metabolic pathways depending on energy demand and fatty acid composition. The predominant pathway involves conversion of fatty acyl CoAs into triglycerides and glycerophospholipids and results in the generation of lipid intermediates including diacylglycerols (DAGs). Alternatively, fatty acids can be directed towards the generation of sphingolipids or converted to acyl-carnitines for transport into the mitochondria for β-oxidation.

Hepatic steatosis occurs when excess FFAs are transported to the liver and/or when increased *de novo* synthesis of triglycerides exceeds the ability of the liver to metabolize or secrete FFAs as very low density lipoprotein. The accumulation of excess FFA in hepatocytes may directly cause lipotoxicity by promoting oxidative stress and activation of inflammatory pathways or may sensitize hepatocytes to mitochondrial dysfunction, oxidative stress, and inflammatory cytokines and adipokines (5). These events will likely lead to simple steatosis and eventually progress to NASH.

NAFLD is frequently observed in patients with type 2 diabetes mellitus and is highly associated with insulin resistance. While the contributing mechanisms involved in the relationship between NAFLD and insulin resistance are unknown, there are several proposed models. One prominent hypothesis suggests that underlying mitochondrial deficiency results in the accumulation of toxic lipid metabolites that can interfere with insulin signaling (6, 7). An alternative hypothesis suggests that increased lipids cause mitochondrial overload, leading to the accumulation of lipid metabolites and reactive oxygen species (ROS) that subsequently cause mitochondrial dysfunction and an insulin resistant state (7, 8). Moreover, elevated ROS and associated reactive derivatives can deplete ATP, NAD and glutathione levels, causing oxidative stress, DNA and protein damage and cell death (9). Studies using serum or liver biopsies from patients with NAFLD have explored metabolic characteristics of NAFLD, and observed altered glutathione, bile acids, carnitine, branched chain amino acids (BCAA) and γ-glutamyl peptides and mouse models of diet-induced obesity show similar overlap in serum and liver-specific metabolites (8, 10–14).

Metabolomics has been used to identify biochemical alterations in cellular systems (15–17). The aim in the current study was to establish a cell-based model of steatosis and apply an unbiased metabolomics approach to determine biochemical signatures associated with steatotic progression and insulin resistance. We achieved this goal by developing a novel,

high throughput method for extracting metabolites from adherent cells. With this method, termed Intact Sample Extraction (ISE), metabolites are extracted and processed for metabolomic analysis, leaving cells attached to the culture plate, preserving the cells for additional analysis and streamlining metabolite extraction. We first examined steatotic transition using the saturated fatty acid palmitate, which is associated with lipid-induced cell toxicity (18, 19). In a separate experiment, we sought to understand the differences between steatosis induced by palmitate and a more physiologically relevant mixture of saturated and unsaturated fatty acids, palmitate and oleate (1:2). Using the ISE method, metabolites analyzed from the lipid-loaded HepaRG cells revealed key metabolic pathways associated with the progression of human NAFLD including insulin resistance, altered mitochondrial metabolism, and oxidative stress.

Methods and Procedures

Cell culture

For the method comparison study, HEK293 cells were seeded at 4×10^4 cells per well in 6-well plates and grown to confluence in EMEM (ATCC, Manassas, VA) supplemented with 10% FBS, 1% Pen/Strep. For method scale-down studies, HepG2 cells were seeded in 6-, 12-, 24- and 96-well formats and expanded to confluence over 48 hours in DMEM supplemented with 10% FBS, glutaMAX I (Life Technologies, Grand Island, NY) and antibiotics. For each experiment, cells were seeded simultaneously using an appropriate number of wells for metabolomic studies and protein analysis. HepaRG cells (Biopredic International, Rennes, France) were seeded at 2.9×10^4 cells per cm^2 in 12-well plates and differentiated as previously described (20).

Metabolite extraction and sample preparation

For method validation, four replicates of HEK293 cells were prepared using the conventional cell scraping and homogenization extraction method. Briefly, cells were rinsed once in PBS, dislodged using a cell scraper and pelleted. Cell pellets were extracted as previously described (15).

Metabolites were extracted from cells at confluence for the method development (4 replicates/condition), method scale down (5 replicates/condition), palmitate timecourse (4 replicates/condition) and palmitate:oleate (3 replicates/condition) experiments. Except where indicated, metabolites were extracted using the ISE method, media was removed, and cells were rinsed once in PBS. Room temperature 80% methanol (20% ultrapure water) was immediately added to the cells, and metabolites were extracted for five minutes at room temperature. The methanol extract was removed and stored at −80°C until processing. Cells for the lipid timecourse experiment were rinsed briefly with PBS and fixed for staining as indicated below. Methanol extracts were evaporated to dryness under a stream of nitrogen gas at 40° C in a Turbovap LV evaporator (Zymark, Hopkinton, MA). The dried extracts were reconstituted in 550 μl methanol:water (80:20) containing recovery standards (D,L-2-fluorophenylglycine, D,L-4-chlorophenylalanine, tridecanoic acid, D6 cholesterol).

Metabolomic profiling

Global metabolomic profiling was carried out on three independent instrument platforms, one gas chromatography/mass spectrometry (GC/MS) and two ultra-high performance liquid chromatography/tandem mass spectrometry (UHPLC/MS/MS²) platforms optimized for either basic or acidic species as previously described (21, 22). Metabolites were identified by automated comparison of the ion features in the experimental samples to a reference library of chemical standard entries that included retention time, molecular weight (m/z), preferred adducts, and in-source fragments as well as their associated MS/MS² spectra. This library allowed the rapid identification of metabolites in the sample with high confidence.

Preparation of fatty acids and lipid loading

Stock solutions of palmitate (200 mM) or oleate (100 mM) (Sigma, St. Louis, MO) were prepared in ethanol or 1.6 mM NaOH solution respectively. Palmitate or a mixture of palmitate:oleate at a ratio of 1:2 were conjugated to albumin in 30% essentially fatty acid free (FAF) BSA solution (Invitrogen, Grand Island, NY) and diluted to 10 mM in Williams E (Invitrogen). Differentiated cells were transferred to media containing 0.5 mM lipid or BSA alone for the indicated times, with media replaced daily.

Triglyceride Accumulation

HepaRG were loaded with 0.1–0.5 mM BSA-conjugated palmitate or palmitate:oleate (1:2) for 48 hours. Samples were rinsed in PBS followed by determination of triglyceride content using the triglyceride assay kit (ZenBio Inc, Research Triangle Park, NC). The optical density was read at 540nm on a Spectramax (Molecular Devices, Sunnyvale, CA) plate reader, and the concentration of glycerol was determined using the following equation: 1M triglyceride = 1M glycerol + fatty acids. The mean concentration of triglyceride and standard deviation were calculated for each sample. A two-tailed t-test was used to calculate significant (p-value   0.05) differences between BSA and lipid-loaded samples at each concentration.

Oil Red O staining

Following metabolite extraction, the cells were rinsed briefly in PBS and stained with Oil Red O. Cells were fixed for at least 1 hour in 4% paraformaldehyde at 4° C and rinsed twice with water. Cells were then stained with 0.5% Oil Red O solution for 20 minutes at RT, washed 2–3 times in water and images were captured on a Ziess Axiovert microscope equipped with a digital camera and supporting IC capture software (The Imaging Source, Charlotte, NC).

ROS Assays

Differentiated HepaRG cells were treated with BSA or palmitate (0.3 or 0.5 mM) for 72 hours in triplicate. ROS production was analyzed using the Image-IT live reactive oxygen detection kit (Invitrogen) using manufacturer's protocol. The mean and standard deviation were calculated and expressed as relative fluorescent units (RFU). Significance was determined by two-tailed t-test, with p   0.05 considered significant.

Insulin-stimulated phosphorylation of AKT

Lipid-loaded HepaRG cells were placed in serum free media for 8 hours, followed by stimulation with recombinant human insulin (Roche Diagnostics, Indianapolis, IN) at 0.1, 1.0, 10 or 100nM for 10 minutes. Samples were rinsed in PBS and lysed in RIPA buffer (150mM NaCl, 50mM Tris, 1% NP-40, 0.5% sodium deoxycholate, 0.1% SDS, 1mM EDTA) supplemented with complete protease inhibitor cocktail (Roche Diagnostics) and HALT phosphatase inhibitor cocktail (Thermo Scientific, Waltham, MA). Protein concentration was determined in the lysates using BCA protein assay reagent (Thermo Scientific). 50 μg of protein was separated on a 4–12% NUPAGE BIS-Tris gel (Life Technologies), transferred to nitrocellulose and blocked in Tris-buffered saline, pH 7.5, 0.1% Tween-20 and 3% FAF BSA for 1 hour. Membranes were rocked at 4° C overnight with phospho or total AKT primary antibody (Cell Signaling Technology, Danvers, MA) at 1:1000 dilution. The membranes were washed three times in TBST for 5 minutes followed by incubation with secondary antibody 1:3000 in 5% milk in TBST (Cell Signaling Technology). After 3 TBST washes, membranes were incubated with Supersignal West Pico chemiluminescence detection reagent (Thermo Scientific), and luminescent signals were captured using a BioRad Gel Documenation system (BioRad laboratories, Hercules, CA).

Statistical Analysis

Missing values for a given metabolite were imputed with the observed minimum detection value based on the assumption that they were below the limits of instrument detection sensitivity. All comparisons were performed using log-transformed data. All samples were normalized to protein as determined by BCA assay (described above). Welch's two sample t-tests or two-way ANOVA with contrasts (palmitate timecourse) were used for comparisons. Multiple comparisons were accounted for with the false discovery rate (FDR) method, and each FDR was estimated using q-values. Biochemicals with $p \leq 0.05$ and $q \leq 0.1$ were considered statistically significant. For convenience of data visualization, raw area counts for each biochemical were re-scaled by dividing the value for a specific biochemical in each sample by the median value for that specific biochemical. Comparisons are represented as fold of change values. Principal Component Analysis (PCA) was performed to characterize the metabolic differences between the palmitate and control groups at each timepoint. For the PCA, each principal component is a linear combination of all metabolites. The coefficients for the first component are determined by those that maximize the variance. The coefficients for the second component are chosen to maximize the variance with the constraint that it is orthogonal to the first component. All statistical analyses were generated using Array Studio software. Array Studio, Array Viewer and Array Server and all other Omicsoft products or service names are registered trademarks or trademarks of Omicsoft Corporation (Research Triangle Park, NC).

Results

Method development and scale down

The ISE method reported here was first compared to a traditional homogenization extraction method of harvested pellets of HEK293 cells. We identified 182 metabolites using the ISE method and 163 using the harvested cell pellet extraction method; 161 metabolites were

common to both methods (Supplemental Figure 1A). The metabolites identified using the ISE method represent a broad range of biochemical classes (Supplemental Figure 1B).

The ability to detect metabolites in multi-well formats was first determined using HepG2 cells plated in various well formats and analyzed by global metabolomics. The well sizes, volume of solvent used for extraction, and the number of cells seeded per well are displayed in Supplemental Table 1. Using the ISE method and non-targeted biochemical profiling, 221 distinct metabolites, matching named structures in our chemical reference library, were identified from a confluent 6-well plate of HepG2 cells (Supplemental Table 1). Not surprising, the average levels of metabolites decreased as the size of the well and total cell number decreased (Supplemental Table 1); likely due to some metabolites to falling below the level of detection by the instrument. Nonetheless, 189 out of 221 metabolites (86%) were detected in the 96-well format when using this extraction method. Furthermore, the cells remained fixed to the plate, allowing them to be utilized in additional cell staining procedures. With the ISE method, it is possible to perform global metabolomics analysis using higher throughput plate formats.

Induction of steatosis in HepaRG cells

To establish conditions that induce steatosis, HepaRG cells were cultured in growth media supplemented with 0.1, 0.3 or 0.5 mM BSA-conjugated palmitate or palmitate:oleate (1:2), or with BSA alone for 48 hours, and triglyceride levels were measured. Increased total triglyceride levels were observed in both lipid treatment conditions. These increases were significant for treatment with 0.3 and 0.5 mM lipid compared to BSA alone (Figure 1A). Using 0.5 mM fatty acid, triglyceride levels were similarly increased for both fatty acid treatments (2.9- and 3.1-fold increases compared to BSA control for palmitate and palmitate:oleate treatments, respectively) (Figure 1A). For subsequent experiments, 0.5 mM fatty acid was used to induce steatosis.

Metabolite profiles of steatotic HepaRG cells

To capture the metabolic transition to steatosis, HepaRG cells were treated with BSA-conjugated palmitate or BSA alone over a 48 hour timecourse. Lipid accumulation was visible in the palmitate-loaded samples within 8 hours and continued to accumulate through the 48 hour timepoint as determined by Oil Red O staining (Figure 1B). Following metabolite extraction, global metabolomic profiling of the palmitate-loaded samples at 8, 16, 24 and 48 hours identified a total of 169 biochemicals (Supplemental Table 2). Principal component analysis (PCA) was used as a way to visualize the samples based on their metabolic profiles. Information from the complete data set was reduced to two principal components. As seen in Figure 1C, palmitate-treated samples separated from BSA samples at all timepoints with the exception of time 0. These data imply that a clear metabolic signature of palmitate-induced steatosis can be obtained in HepaRG cells. In fact, we observed distinct metabolic profiles of palmitate-treated HepaRG cells over 48 hours in the transition to steatosis (Figures 1–5).

However, given the lipotoxic effects of prolonged exposure to saturated fatty acids, including palmitate, we performed an independent follow-up study using palmitate alone or

a physiological mixture of saturated and unsaturated fatty acids (palmitate and oleate, 1:2) (Table 1). Based on the results of the palmitate timecourse, we selected 8 and 48 hour treatment timepoints for the follow-up study. While distinct metabolic profiles were observed for each steatotic treatment, both palmitate and palmitate:oleate treated HepaRG cells demonstrated changes in metabolites that were indicative of altered lipid and energy metabolism and insulin resistance. The results from both studies are presented in parallel below.

As expected from fatty acid loading, lipid metabolism was significantly altered in both metabolomic studies, particularly evident through observed changes in carnitine metabolism. Treatment with palmitate or palmitate:oleate led to reduced levels of carnitine (Figure 2A and Table 1) while acylcarnitines including butyrylcarnitine, propionlycarnitine and oleoylcarnitine were significantly elevated (Figure 2B and Table 1). Acetyl CoA was also significantly elevated with both fatty acid treatments at 8 hours (Table 1). However, reduced levels of coenzyme A were observed only with palmitate treatment at the 48 h time point (Figure 2C, Table 1).

Significant changes in energy metabolism were consistently observed between palmitate-treated and BSA control samples. Carbohydrate metabolism contributions to the TCA cycle during the 48 h of palmitate treatment are shown in Figure 3. The product of anaerobic glycolysis, lactate, and the TCA cycle intermediates, cis-aconitate, fumarate and malate were significantly higher in palmitate-loaded samples for all timepoints. Citrate was significantly elevated at 8, 16 and 24h, and alpha-ketoglutarate was elevated at 16 and 48 h with palmitate treatment. Elevated lactate and TCA cycle intermediates were also observed in palmitate:oleate-treated cells at the 48 hour timepoint (Table 1). The BCAAs, isoleucine, leucine, and valine, were significantly elevated in palmitate- and in palmitate:oleate-treated cells at 48 hours (Figure 4A and Table 1), indicating possible anaplerotic contributions to the TCA cycle.

In palmitate-treated samples, DAG and monoacylglycerols (MAG) were significantly elevated (Figure 4B, Supplemental Table 2 and Table 1). The DAGs, 1,2-dipalmitoylglycerol and 1,3-dipalmitoylglycerol were elevated within 8 hours of palmitate treatment (Figure 4B and Table 1) whereas increased MAG levels were observed at 48 hours (Supplemental Table 2, Table 1). In contrast, DAG and MAG levels were not significantly altered in palmitate:oleate-treated cells (Table 1). Levels of the ceramide precursor, sphingosine, were elevated in both palmitate- (Figure 4C and Table 1) and palmitate:oleate-treated cells (Table 1).

Bile acids (BA) are involved in glucose homeostasis through interaction with BA receptors FXR (Farnesoid X receptor) and TGR5 (23, 24). The primary bile acid taurocholate was significantly reduced compared to BSA controls within 8 hours of palmitate treatment in both studies (Figure 1D and Table 1). In contrast, taurocholate was unaltered by palmitate:oleate treatment (Table 1).

Biochemicals involved in glutathione metabolism, including cystathionine and S-adenosylhomocysteine (SAH), were altered with palmitate treatment in both studies (Figure

5A, Table 1, Supplemental Table 2). Several other biochemicals of glutathione metabolism were significant in the palmitate timecourse study. Beginning at 24 hours, glutathione (GSH) levels in palmitate-treated samples were reduced compared to BSA and were significant at 48 hours (Figure 5B). Gamma-glutamylthreonine was transiently elevated by palmitate at 8–24h timepoints, with gamma-glutamylleucine elevated later at 16h and 24h (Figure 5B). Overall, glutathione metabolism was not significantly altered in HepaRG cells treated with palmitate:oleate.

ROS Assays

To determine the extent of ROS generation in palmitate-treated cells, we labeled cells with carboxy-H_2DCFDA fluorescein. This cell-permeable fluorogenic marker is readily oxidized by ROS into a fluorescent product. Cells were treated with BSA, 0.3 or 0.5 mM palmitate; tert buytl hydroperoxide (100 μM, 1 hour) was used as a positive control. Compared to BSA control samples, ROS were elevated 1.5 fold ($p<0.036$) and 1.7 fold ($p<0.025$) in the presence of 0.3 mM or 0.5 mM palmitate, respectively (Figure 5C). These data support the metabolic indications of oxidative stress in the palmitate induced steatotic model as predicted by the metabolic signatures.

Lipid-induced decrease in insulin-stimulated phosphorylation of AKT

Elevated mitochondrial β-oxidation and increased oxidative and anaplerotic contributions to the TCA cycle are reported to generate lipid-derived metabolites and reactive oxygen species (ROS) in human NAFLD and hepatocyte cultures, decreasing the ability of insulin to stimulate proximal signaling events (25). To test the hypothesis of lipid-induced alterations in insulin signaling, BSA or palmitate-loaded HepaRG cells were treated with increasing concentrations of insulin (0.1–100 nM) for 10 minutes followed by analysis of total and phosphorylated AKT by immunoblotting. In BSA control samples, insulin stimulation resulted in the expected concentration-dependent increase in AKT phosphorylation at serine 473. In contrast, insulin-stimulated phosphorylation of AKT was reduced in palmitate-loaded cells by ~30% at the highest concentrations (data not shown). Total AKT levels remained constant for all treatment conditions. This finding supports our metabolomic data indicating an insulin resistant phenotype in palmitate-loaded HepaRG cells.

Discussion

In this study, we characterized a cell-based model of lipid-induced hepatic steatosis using HepaRG cells treated with palmitate alone or a combination of palmitate and oleate. We established a protocol to extract metabolites from intact cells in a multi-well format, identified metabolic signatures of steatotic progression induced by palmitate and palmitate:oleate, and validated several of these metabolic profiles with biological assays. Our data from two independent metabolomic studies revealed changes in metabolites related to energy metabolism, insulin resistance and oxidative stress, which are key biochemical processes known to be involved in steatosis and NASH. Importantly, the distinct metabolic signatures identified using this *in vitro* cell model, including elevated levels of lipid metabolites, TCA cycle intermediates and BCAAs and reduced levels of carnitine and

glutathione, recapitulates biochemical alterations observed in serum and liver tissue from human NAFLD patients and in animal models of NAFLD (10–12, 14, 26–30).

Elevated DAG levels in liver biopsies from NAFLD patients and animal models of NAFLD are associated with hepatic lipotoxicity (31). Elevated DAG has also been implicated in the development of hepatic insulin resistance through activation of protein kinase C ε (32). We observed a significant accumulation of DAG and MAG metabolites in palmitate-treated HepaRG cells, consistent with studies describing insulin resistant and lipotoxic phenotypes in response to saturated fatty acids (18, 19, 33). Metabolic indications of oxidative stress in palmitate-treated HepaRG cells were supported by ROS assays. In contrast, oleate protects against palmitate-induced lipotoxicity by targeting palmitate for triglyceride synthesis (33, 34). In our palmitate:oleate-treated steatotic model, DAG and MAG levels were not significantly altered, suggesting that oleate is protective against accumulation of these lipid metabolites. However, elevated levels of sphingolipid suggest that the ceramide signaling pathway may be altered in palmitate:oleate-treated HepaRG cells. Ceramide levels are increased in insulin-resistant humans, and this has been attributed to ceramide impairment of insulin-stimulated phosphorylation of Akt (35). These data demonstrate that different fatty acids or combinations of fatty acids may induce insulin resistance through distinct mechanisms.

Elevated acetyl CoA and concomitant decrease in carnitine levels in the steatotic HepaRG cells, suggest that processing of fatty acids through β-oxidation is occurring at early timepoints but may be limited with prolonged lipid treatment due to eventual depletion of free carnitine. Carnitine supplementation has been explored for its ability to promote β-oxidation of fatty acids and reduce steatosis in rodent models (36). Without carnitine supplementation, fatty acids may be preferentially partitioned towards alternative metabolic pathways that could contribute to the generation of toxic lipid metabolites (8). Interestingly, palmitoylcarnitine was elevated in palmitate-treated cells, whereas both palmitoylcarnitine and oleoylcarnitine were elevated in palmitate:oleate conditions. These incompletely oxidized fatty acids further suggest altered β-oxidation. In a mouse model of NAFLD, metabolomic analysis revealed depletion of carnitine in liver tissue but not in serum (14). In a separate metabolomic study, elevated levels of circulating carnitine species including free carnitine, butyrylcarnitine and methylbutyrylcarnitine, were observed in plasma from NAFLD patients (10). The results in liver tissue are consistent with our findings in the two steatotic cell treatment conditions, and emphasize that plasma/serum metabolites reflect the net result of all organs/tissues rather than organ/tissue-specific alterations.

A recent study analyzing mitochondrial oxidative metabolism in the liver of individuals with NAFLD demonstrates that elevated hepatic triglyceride is associated with higher flux in the TCA cycle and elevated anaplerotic TCA cycle contributions from pyruvate cycling and gluconeogenesis (26). In the present study, we observed an increase in lactate and TCA cycle intermediates in response to palmitate, suggesting increased TCA cycle activity in this condition. This effect may be less severe or delayed in palmitate:oleate conditions as TCA cycle intermediates were not elevated until 48 h, and lactate was not significantly altered.

High levels of BCAAs, which include the essential amino acids valine, leucine, isoleucine and their metabolites, are associated with insulin resistance (28, 37). Elevated BCAAs have been observed in patients with obesity, type 2 diabetes and NAFLD (10, 28, 37, 38) and are strong candidates in predicting insulin sensitivity (38) and monitoring disease progression and response to therapeutic intervention (28, 37). Consistent with these clinical observations and with the altered TCA cycle activity in this model, we observed elevated levels of BCAAs in both fatty acid-loaded conditions, suggesting anaplerotic contributions to the TCA cycle. The BCAA levels in palmitate:oleate-treated cells increased at 48 h, which is consistent with the delayed TCA cycle effect in that condition. When taken in concert, the metabolic indications of impaired β-oxidation and increased TCA cycle activity through anaplerotic contributions, suggest clear mitochondrial abnormalities in both fatty acid-loaded conditions.

In addition to their role in dietary lipid absorption and cholesterol homeostasis, BAs are signaling molecules that play a role in glucose and lipid metabolism (24). Unlike DAGs and ceramide, BA signaling has been shown to improve insulin sensitivity by modulating triglyceride, cholesterol and glucose homeostasis (39). Lower levels of the BA taurocholate are associated with early stage insulin resistance in mice (40). Our observation of reduced taurocholate levels in palmitate-treated HepaRG cells may indicate the onset of an insulin-resistant phenotype. In contrast to our findings, increased levels of bile acids were reported in steatotic liver tissues (12). These opposite effects may be due to sample type differences (HepaRG cells used in our studies compared to human liver tissue), although additional studies are needed to clarify the role of BA signaling in this steatotic HepaRG cell model. Regardless, the data suggest that dysregulation of BA homeostasis is associated with insulin resistance and steatosis and may contribute to the pathogenesis of NAFLD,

In this study, we used a novel method to extract metabolites from intact cells and performed an unbiased metabolomics approach to examine global changes in hepatocyte-like cells during steatotic progression induced by fatty acids. With this approach, we identified key biochemical signatures related to steatosis and NAFLD, including altered mitochondrial metabolism, insulin resistance and oxidative stress. These profiles support many of the reported biochemical alterations observed in animal models of NAFLD and importantly are consistent with metabolomic signatures obtained with clinically relevant human liver samples and serum from patients with varying degrees of fatty liver disease. Our results demonstrate the suitability and utility of this steatotic cell model to further investigate steatosis and insulin resistance and represent a novel platform for drug development and preclinical toxicity studies.

Supplementary Material

Refer to Web version on PubMed Central for supplementary material.

Acknowledgments

References

1. Erickson SK. Nonalcoholic fatty liver disease. J Lipid Res. 2009 Apr; 50(Suppl):S412–6. [PubMed: 19074370]

2. Dunn W, Schwimmer JB. The obesity epidemic and nonalcoholic fatty liver disease in children. Curr Gastroenterol Rep. 2008 Feb; 10(1):67–72. [PubMed: 18417045]

3. Angulo P. Nonalcoholic fatty liver disease. N Engl J Med. 2002 Apr 18; 346(16):1221–31. [PubMed: 11961152]

4. Wei Y, Rector RS, Thyfault JP, Ibdah JA. Nonalcoholic fatty liver disease and mitochondrial dysfunction. World J Gastroenterol. 2008 Jan 14; 14(2):193–9. [PubMed: 18186554]

5. Dowman JK, Tomlinson JW, Newsome PN. Pathogenesis of non-alcoholic fatty liver disease. QJM. 2010 Feb; 103(2):71–83. [PubMed: 19914930]

6. Smith BW, Adams LA. Nonalcoholic fatty liver disease and diabetes mellitus: pathogenesis and treatment. Nat Rev Endocrinol. 2011 Aug; 7(8):456–65. [PubMed: 21556019]

7. Savage DB, Petersen KF, Shulman GI. Disordered lipid metabolism and the pathogenesis of insulin resistance. Physiol Rev. 2007 Apr; 87(2):507–20. [PubMed: 17429039]

8. Koves TR, Ussher JR, Noland RC, Slentz D, Mosedale M, Ilkayeva O, et al. Mitochondrial overload and incomplete fatty acid oxidation contribute to skeletal muscle insulin resistance. Cell Metab. 2008 Jan; 7(1):45–56. [PubMed: 18177724]

9. Rolo AP, Teodoro JS, Palmeira CM. Role of oxidative stress in the pathogenesis of nonalcoholic steatohepatitis. Free Radic Biol Med. 2012 Jan 1; 52(1):59–69. [PubMed: 22064361]

10. Kalhan SC, Guo L, Edmison J, Dasarathy S, McCullough AJ, Hanson RW, et al. Plasma metabolomic profile in nonalcoholic fatty liver disease. Metabolism. 2011 Mar; 60(3):404–13. [PubMed: 20423748]

11. Pilvi TK, Seppanen-Laakso T, Simolin H, Finckenberg P, Huotari A, Herzig KH, et al. Metabolomic changes in fatty liver can be modified by dietary protein and calcium during energy restriction. World J Gastroenterol. 2008 Jul 28; 14(28):4462–72. [PubMed: 18680224]

12. Garcia-Canaveras JC, Donato MT, Castell JV, Lahoz A. A comprehensive untargeted metabonomic analysis of human steatotic liver tissue by RP and HILIC chromatography coupled to mass spectrometry reveals important metabolic alterations. J Proteome Res. 2011 Oct 7; 10(10): 4825–34. [PubMed: 21830829]

13. de Wit NJ, Afman LA, Mensink M, Muller M. Phenotyping the effect of diet on non-alcoholic fatty liver disease. Journal of hepatology. 2012 Dec; 57(6):1370–3. [PubMed: 22796155]

14. Kim HJ, Kim JH, Noh S, Hur HJ, Sung MJ, Hwang JT, et al. Metabolomic analysis of livers and serum from high-fat diet induced obese mice. J Proteome Res. 2011 Feb 4; 10(2):722–31. [PubMed: 21047143]

15. Vulimiri SV, Misra M, Hamm JT, Mitchell M, Berger A. Effects of mainstream cigarette smoke on the global metabolome of human lung epithelial cells. Chem Res Toxicol. 2009 Mar 16; 22(3): 492–503. [PubMed: 19161311]

16. Watson M, Roulston A, Belec L, Billot X, Marcellus R, Bedard D, et al. The small molecule GMX1778 is a potent inhibitor of NAD+ biosynthesis: strategy for enhanced therapy in nicotinic acid phosphoribosyltransferase 1-deficient tumors. Mol Cell Biol. 2009 Nov; 29(21):5872–88. [PubMed: 19703994]

17. Wetmore DR, Joseloff E, Pilewski J, Lee DP, Lawton KA, Mitchell MW, et al. Metabolomic profiling reveals biochemical pathways and biomarkers associated with pathogenesis in cystic fibrosis cells. J Biol Chem. 2010 Oct 1; 285(40):30516–22. [PubMed: 20675369]

18. Malhi H, Bronk SF, Werneburg NW, Gores GJ. Free fatty acids induce JNK-dependent hepatocyte lipoapoptosis. J Biol Chem. 2006 Apr 28; 281(17):12093–101. [PubMed: 16505490]

19. Nakamura S, Takamura T, Matsuzawa-Nagata N, Takayama H, Misu H, Noda H, et al. Palmitate induces insulin resistance in H4IIEC3 hepatocytes through reactive oxygen species produced by mitochondria. J Biol Chem. 2009 May 29; 284(22):14809–18. [PubMed: 19332540]

20. Kanebratt KP, Andersson TB. Evaluation of HepaRG cells as an in vitro model for human drug metabolism studies. Drug Metab Dispos. 2008 Jul; 36(7):1444–52. [PubMed: 18385292]

21. Evans AM, DeHaven CD, Barrett T, Mitchell M, Milgram E. Integrated, nontargeted ultrahigh performance liquid chromatography/electrospray ionization tandem mass spectrometry platform for the identification and relative quantification of the small-molecule complement of biological systems. Anal Chem. 2009 Aug 15; 81(16):6656–67. [PubMed: 19624122]

22. Brown MV, McDunn JE, Gunst PR, Smith EM, Milburn MV, Troyer DA, et al. Cancer detection and biopsy classification using concurrent histopathological and metabolomic analysis of core biopsies. Genome Med. 2012; 4(4):33. [PubMed: 22546470]

23. Zhang Y, Lee FY, Barrera G, Lee H, Vales C, Gonzalez FJ, et al. Activation of the nuclear receptor FXR improves hyperglycemia and hyperlipidemia in diabetic mice. Proc Natl Acad Sci U S A. 2006 Jan 24; 103(4):1006–11. [PubMed: 16410358]

24. Hylemon PB, Zhou H, Pandak WM, Ren S, Gil G, Dent P. Bile acids as regulatory molecules. J Lipid Res. 2009 Aug; 50(8):1509–20. [PubMed: 19346331]

25. Chavez JA, Summers SA. A ceramide-centric view of insulin resistance. Cell Metab. 2012 May 2; 15(5):585–94. [PubMed: 22560211]

26. Sunny NE, Parks EJ, Browning JD, Burgess SC. Excessive hepatic mitochondrial TCA cycle and gluconeogenesis in humans with nonalcoholic fatty liver disease. Cell Metab. 2011 Dec 7; 14(6): 804–10. [PubMed: 22152305]

27. Sunny Nishanth E, Parks Elizabeth J, Browning Jeffrey D, Burgess Shawn C. Excessive Hepatic Mitochondrial TCA Cycle and Gluconeogenesis in Humans with Nonalcoholic Fatty Liver Disease. Cell metabolism. 2011; 14(6):804–10. [PubMed: 22152305]

28. Newgard CB, An J, Bain JR, Muehlbauer MJ, Stevens RD, Lien LF, et al. A branched-chain amino acid-related metabolic signature that differentiates obese and lean humans and contributes to insulin resistance. Cell Metab. 2009 Apr; 9(4):311–26. [PubMed: 19356713]

29. Gorden DL, Ivanova PT, Myers DS, McIntyre JO, VanSaun MN, Wright JK, et al. Increased diacylglycerols characterize hepatic lipid changes in progression of human nonalcoholic fatty liver disease; comparison to a murine model. PLoS One. 2011; 6(8):e22775. [PubMed: 21857953]

30. Yetukuri L, Katajamaa M, Medina-Gomez G, Seppanen-Laakso T, Vidal-Puig A, Oresic M. Bioinformatics strategies for lipidomics analysis: characterization of obesity related hepatic steatosis. BMC Syst Biol. 2007; 1:12. [PubMed: 17408502]

31. Neuschwander-Tetri BA. Hepatic lipotoxicity and the pathogenesis of nonalcoholic steatohepatitis: the central role of nontriglyceride fatty acid metabolites. Hepatology. 2010 Aug; 52(2):774–88. [PubMed: 20683968]

32. Jornayvaz FR, Shulman GI. Diacylglycerol activation of protein kinase Cepsilon and hepatic insulin resistance. Cell Metab. 2012 May 2; 15(5):574–84. [PubMed: 22560210]

33. Montell E, Turini M, Marotta M, Roberts M, Noe V, Ciudad CJ, et al. DAG accumulation from saturated fatty acids desensitizes insulin stimulation of glucose uptake in muscle cells. Am J Physiol Endocrinol Metab. 2001 Feb; 280(2):E229–37. [PubMed: 11158925]

34. Wei Y, Wang D, Pagliassotti MJ. Saturated fatty acid-mediated endoplasmic reticulum stress and apoptosis are augmented by trans-10, cis-12-conjugated linoleic acid in liver cells. Mol Cell Biochem. 2007 Sep; 303(1–2):105–13. [PubMed: 17426927]

35. Adams JM 2nd, Pratipanawatr T, Berria R, Wang E, DeFronzo RA, Sullards MC, et al. Ceramide content is increased in skeletal muscle from obese insulin-resistant humans. Diabetes. 2004 Jan; 53(1):25–31. [PubMed: 14693694]

36. Xia Y, Li Q, Zhong W, Dong J, Wang Z, Wang C. L-carnitine ameliorated fatty liver in high-calorie diet/STZ-induced type 2 diabetic mice by improving mitochondrial function. Diabetol Metab Syndr. 2011; 3:31. [PubMed: 22082204]

37. Newgard CB. Interplay between Lipids and Branched-Chain Amino Acids in Development of Insulin Resistance. Cell Metab. 2012 May 2; 15(5):606–14. [PubMed: 22560213]

38. McCormack SE, Shaham O, McCarthy MA, Deik AA, Wang TJ, Gerszten RE, et al. Circulating branched-chain amino acid concentrations are associated with obesity and future insulin resistance in children and adolescents. Pediatr Obes. 2012 Sep 7.

39. Wei J, Qiu de K, Ma X. Bile acids and insulin resistance: implications for treating nonalcoholic fatty liver disease. J Dig Dis. 2009 May; 10(2):85–90. [PubMed: 19426389]

40. Li LO, Hu YF, Wang L, Mitchell M, Berger A, Coleman RA. Early hepatic insulin resistance in mice: a metabolomics analysis. Mol Endocrinol. 2010 Mar; 24(3):657–66. [PubMed: 20150186]
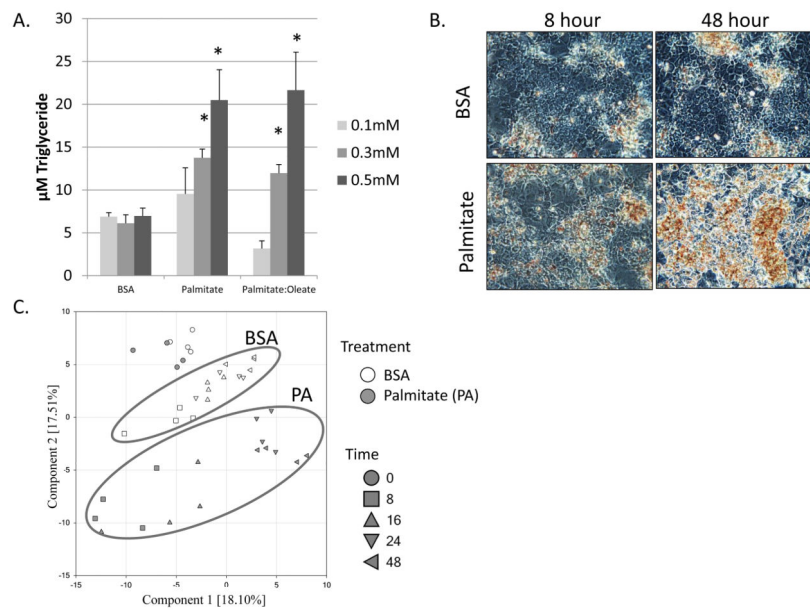
Figure 1. Characterization of fatty acid-loaded HepaRG cells

A) Differentiated HepaRG cells were treated with BSA alone or with the indicated concentrations of palmitate or palmitate:oleate (1:2) for 48 hours prior to assaying triglyceride content. Asterisks indicate a significant (p 0.05) difference compared to BSA alone. B) Differentiated HepaRG cells were incubated with BSA (top panels) or BSA-conjugated palmitate (bottom panels) for 8 or 48 hours. Cells were briefly exposed to methanol to extract metabolites followed by fixation and staining with 0.5% Oil Red O. Representative images revealing the accumulation of lipid droplets (red staining) were captured on a Ziess Axiovert microscope equipped with a digital camera and supporting IC capture software. C) Principal component analysis based on the metabolic profiles of BSA (open shapes) and palmitate-treated (solid shapes) samples over time. Two principal components were used (Component 1, x-axis; Component 2, y-axis), and the percent variance for each component is shown. Each time is represented by a different shape (0, circle; 8 h, square; 16 h, upward pointing triangle; 24 h, downward pointing triangle; 48 h, left pointing triangle). The inclusion of the samples in each group (BSA or palmitate treatment) is indicated by the large ovals.
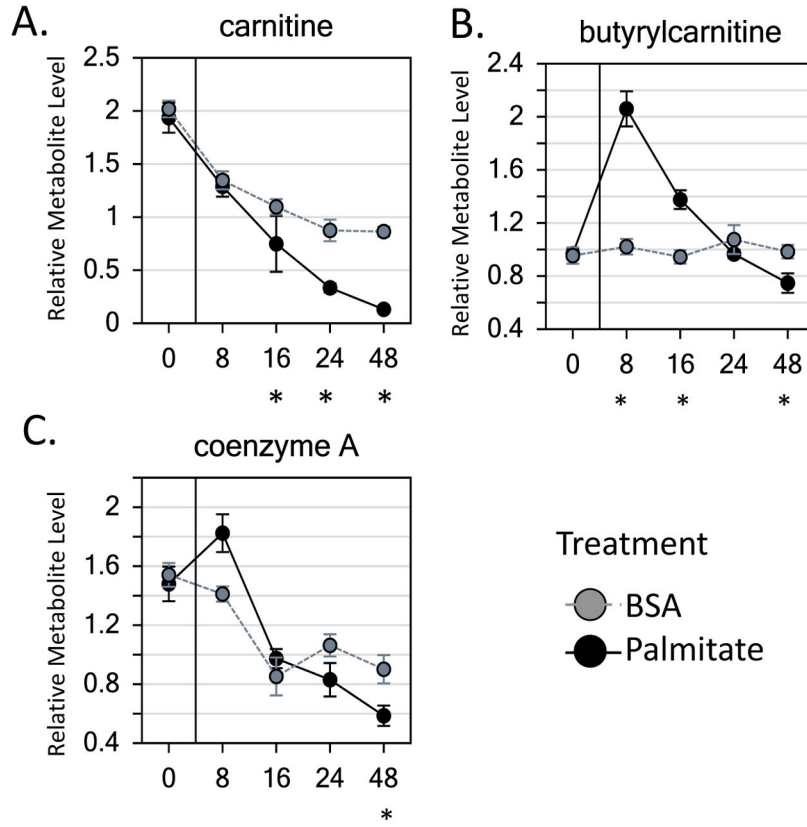
Figure 2. Lipid metabolism

A) Line plot view of carnitine. For the line plot, the mean relative metabolite level is shown for BSA (gray) and palmitate-treated (black) samples at the indicated time points. The x-axis represents the treatment time. The y-axis represents the relative level of the metabolite. Asterisks indicate a significant difference (p 0.05, q 0.1) between palmitate treatment and BSA control at the given time. Error bars indicate one standard error (SE). B) Line plot view of butyrylcarnitine. C) Line plot view of coenzyme A.
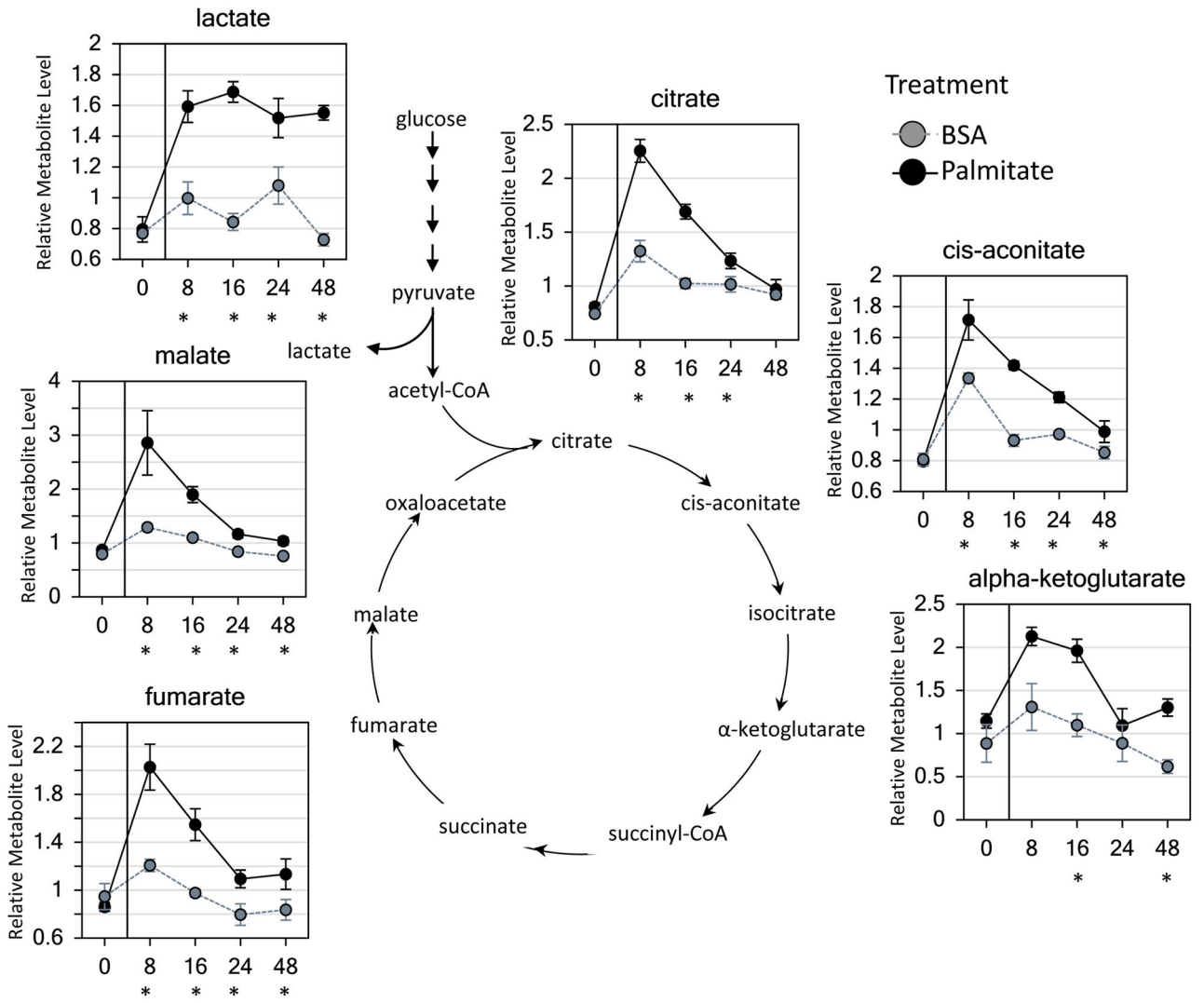
Figure 3. Effect of palmitate on glycolytic contribution to the TCA cycle
Metabolites involved in glycolysis and the TCA cycle are indicated by line plots. The mean relative metabolite level is shown for BSA (gray) and palmitate-treated (black) samples at each time point. The x-axis represents the treatment time. The y-axis represents the relative level of the metabolite. Asterisks indicate a significant difference (p 0.05, q 0.1) between palmitate treatment and BSA control at the given time. Error bars indicate one SE.
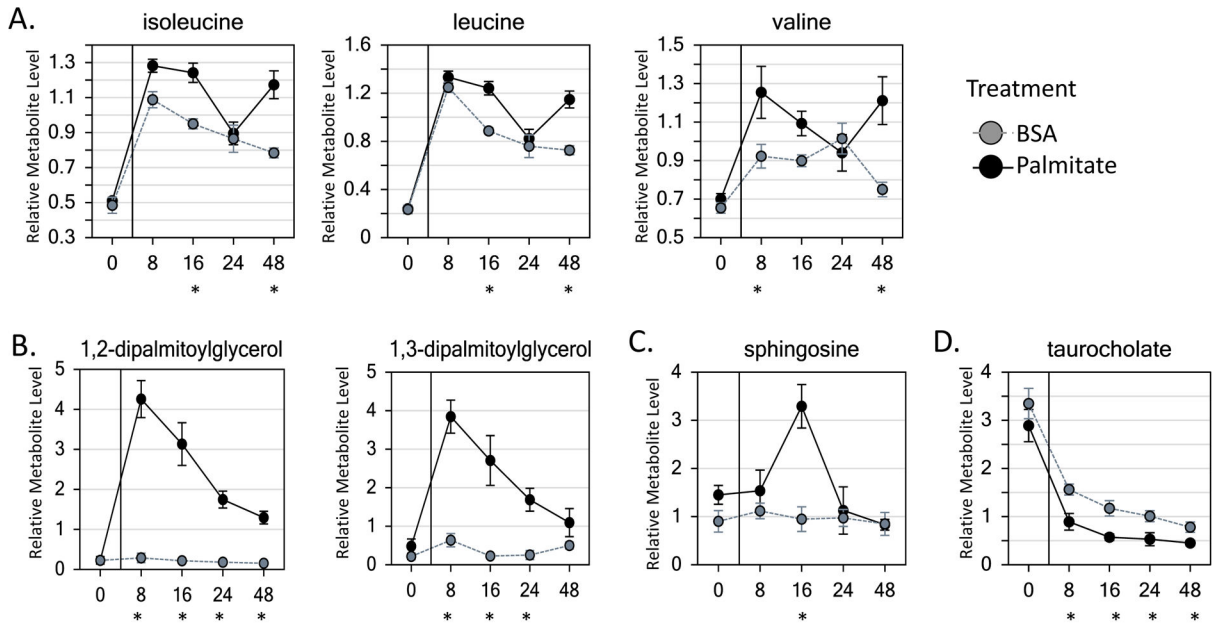
Figure 4. Metabolic indications of insulin resistance

A) Line plot view of the branched chain amino acids isoleucine, leucine and valine. The mean relative metabolite level is shown for BSA (gray) and palmitate-treated (black) samples at each time point. The x-axis represents the treatment time. The y-axis represents the relative level of the metabolite. Asterisks indicate a significant difference (p 0.05, q 0.1) between palmitate treatment and BSA control at the given time. Error bars indicate one SE. B) Line plot view of the diacylglycerols, 1,2-dipalmitoylglycerol and 1,3-dipalmitoylglycerol. C) Line plot view of the ceramide precursor, sphingosine. D) Line plot view of the bile acid, taurocholate.
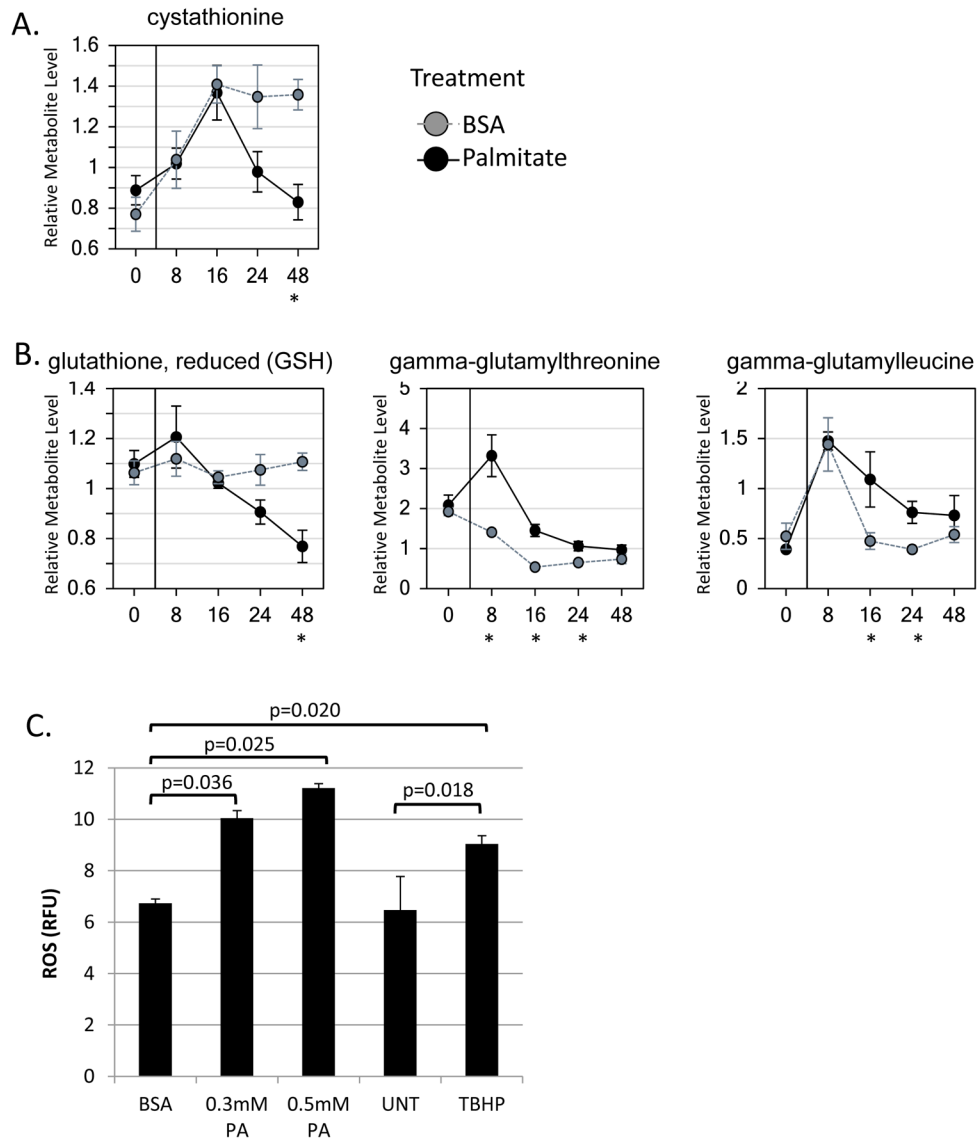
Figure 5. Glutathione metabolism and oxidative stress

A) Line plot view of cystathionine. The mean relative metabolite level is shown for BSA (gray) and palmitate-treated (black) samples at each time point. The x-axis represents the treatment time. The y-axis represents the relative level of the metabolite. Asterisks indicate a significant difference (p 0.05, q 0.1) between palmitate treatment and BSA control at the given time. Error bars indicate one SE. B) Line plot views of reduced glutathione (GSH), gamma-glutamylthreonine and gamma-glutamylleucine. C) HepaRG cells were untreated (UNT), loaded with BSA or BSA-conjugated palmitate (PA) at 0.3 or 0.5 mM for 72 hours, or exposed to 100 μM TBHP (positive control). The mean level of reactive oxygen species (ROS) detected using carboxy-H_2DCFDA fluorescein is shown (n=3) and expressed as relative fluorescent units (RFU). Error bars represent standard deviation. Statistically significant changes are indicted with their calculated p values.

Table 1

Selected metabolites altered in palmitate- and palmitate:oleate-treated HepaRG cells at 8 and 48 hours

Metabolite values are expressed as fold of change for the indicated condition relative to BSA control. Bold values are significant with p 0.05 and q 0.1

Classification	Biochemical Name	Fold Change Relative to BSA Control			
		Palmitate		Palmitate:Oleate	
		8 Hours	48 Hours	8 Hours	48 Hours
	carnitine	**0.58**	**0.35**	**0.27**	**0.56**
	3-dehydrocarnitine	0.83	0.67	0.87	1.46
	acetylcarnitine	1.23	**0.64**	1.44	1.16
Carnitine metabolism	palmitoylcarnitine	**2.88**	**2.7**	1.86	1.38
	oleoylcarnitine	1.01	0.86	**2.37**	**2.83**
	propionylcarnitine	1.38	1.23	1.21	1.39
	butyrylcarnitine	**2.18**	**3.43**	**2.41**	**2.48**
Pantothenate and CoA metabolism	coenzyme A	0.93	0.63	0.92	1.02
	acetyl CoA	**1.99**	0.94	**1.78**	0.78
Glycolysis, gluconeogenesis, pyruvate metabolism	glucose-6-phosphate (G6P)	0.86	1.15	0.95	1.69
	glucose	**0.58**	0.93	0.81	**1.3**
	lactate	**1.37**	**1.86**	1.11	1.54
	citrate	**1.45**	1.38	1.39	**1.98**
	alpha-ketoglutarate	1.25	1.4	0.91	1.45
TCA cycle	succinate	**0.67**	1.36	0.77	1.46
	fumarate	1.3	1.38	1.05	1.78
	malate	**1.52**	1.27	1.13	**1.73**
	isoleucine	**0.81**	**1.86**	0.91	**1.65**
	leucine	0.99	**2.1**	0.98	**1.82**
Valine, leucine and isoleucine metabolism	valine	**0.83**	1.45	0.87	**1.4**
	2-methylbutyrylcarnitine (C5)	1.13	1.34	1.01	1.25
	isovalerylcarnitine	1.27	**2.42**	1.25	1.96

Classification	Biochemical Name	Fold Change Relative to BSA Control			
		Palmitate		Palmitate:Oleate	
		8 Hours	48 Hours	8 Hours	48 Hours
Monoacylglycerol	1-pentadecanoylglycerol (1-monopentadecanoin)	1.07	**1.37**	1.02	1.4
	1-heptadecanoylglycerol (1-monoheptadecanoin)	0.9	**1.37**	0.85	1.17
	1-palmitoylglycerol (1-monopalmitin)	0.86	**1.39**	0.84	1.14
	2-palmitoylglycerol (2-monopalmitin)	0.91	1.58	0.89	1.07
	1-stearoylglycerol (1-monostearin)	0.89	**1.41**	0.83	1.14
	2-stearoylglycerol (2-monostearin)	0.85	**1.64**	0.81	1.11
	1-oleoylglycerol (1-monoolein)	0.89	1.19	0.89	1.3
	1-behenoylglycerol (1-monobehenin)	0.95	**1.43**	0.91	1.08
Diacylglycerol	1,2-dipalmitoylglycerol	**9.76**	**13.28**	1.29	1.44
	1,3-dipalmitoylglycerol	2.59	**5.93**	0.84	1.59
Sphingolipid	sphingosine	1.84	0.98	1.36	**1.73**
	palmitoyl sphingomyelin	0.99	0.87	1.05	**1.46**
Bile acid metabolism	taurocholate	0.56	**0.28**	0.64	0.8
	taurochenodeoxycholate	**0.57**	**0.26**	0.83	1.04
Glutathione metabolism	cysteine	**0.7**	1	0.8	1
	cystathionine	0.8	**0.6**	0.9	1.1
	S-adenosylhomocysteine (SAH)	1.1	**0.5**	1.3	1.5
	glutathione, reduced (GSH)	0.97	0.92	1.03	1.05
	S-methylglutathione	0.85	0.95	**0.5**	1.19
	5-oxoproline	1	0.81	1.65	1.42
	glutathione, oxidized (GSSG)	0.79	0.7	0.97	1.29
	S-lactoylglutathione	**2.42**	1.59	0.89	1.27